Thermoluminescence, Photoluminescence and Optically Stimulated Luminescence Characteristics of $CaSO_4$:Eu Phosphor: An Experimental and Density Functional Theory (DFT) Investigation

Nandkumar T. Mandlik[a*], Sachin R. Rondiya[b], Nelson Y. Dzade[b], M. S. Kulkarni[c], P. D. Sahare[d], B. C. Bhatt[e] , S. D. Dhole[f]

[a]Department of Physics, Fergusson College, Savitribai Phule Pune University, Pune 411004, Maharashtra, India.

[b]The School of Chemistry, Cardiff University, Cardiff, CF10 3AT, Wales, UK

[c]Health Physics Division, BARC, Mumbai 400085, Maharashtra, India

[d]Department of Physics and Astrophysics, University of Delhi, Delhi 110007, India.

[e]Ex-BARC Scientist, B-6, Ameya Cooperative Housing Society, Sector 9-A, Vashi, Navi Mumbai 400703, India.

[f]Department of Physics, Savitribai Phule Pune University, Pune 411007, Maharashtra, India.

[*]Corresponding author E-mail: nandkumar.mandlik@fergusson.edu, ntmandlik@gmail.com

Abstract

The $CaSO_4$:Eu phosphor in nanocrystalline form was obtained by chemical method. The sample was annealed at various temperatures and quenched. The structural, electronic and optical properties are studied using various experimental techniques. As synthesized $CaSO_4$:Eu particles have nanorod shapes with diameter of ~15 nm and length of ~250 nm. After annealing (at around 900 °C) a significant increase in their size (~2-4 μm) with phase transformation from hexagonal to orthorhombic was observed. Thermoluminescence (TL) and optically stimulated luminescence (OSL) intensities were found to increase with temperatureup to 900 °C and decrease thereafter for 1 Gy of test dose of β-rays from ^{90}Sr-^{90}Yr source. However, the maximum OSL sensitivity was found to be more than that of $CaSO_4$:Eu microcrystalline phosphor (prepared by acid recrystallization method) contrary to the usually found in the literature but much less than that of commercially available α-Al_2O_3:C phosphor. The activation energy for thermally assisted OSL process was found to be 0.0572 ± 0.0028 eV. The dose ranges of TL and OSL response was found from 0.04 Gy to 100 Gy and 0.02 Gy to 100 Gy, respectively. The experimental results are also correlated with computational calculations based on density functional theory (DFT). The crystal structures and electronic structures of both hexagonal and orthorhombic $CaSO_4$ and $CaSO_4$:Eu materials show that they are direct bandgap (5.67−5.86 eV) insulators, with Ca^{2+}

substitution by Eu^{2+} found to introduce donor states in the bandgap near Fermi level and the valence band edge of $CaSO_4$ on doping with Eu^{2+} impurity ions.

1. Introduction

High-energy radiations, such as, X-rays, γ-rays, β-rays, neutrons, swift heavy ions, etc., are hazardous to living beings [1]. High doses of such radiation could cause radiation burns, cancer and even death. However, the usage of sources of such radiations cannot be completely avoided in day-to-day life as they are used for medical diagnostic purposes, in food processing and preservation, for energy generation using nuclear reactors and in scientific research and developments. But for taking protective measures for radiation workers and others, it is necessary to measure and monitor doses of such radiations. TL is widely used as a tool for applications in personnel and environmental dosimetry, medical dosimetry, archaeological and geological dating, space dosimetry, etc. [2-4]. It has been found that some thermoluminescence dosimeter (TLD) materials may change their thermoluminescence (TL) characteristics on annealing at different temperatures and/or on heating and cooling several times during readouts for its reuse and could lose their reusability [5]. There is decrease in the efficiency of luminescence due to this which is generally termed as thermal quenching [6]. This difficulty can be overcome in the advanced technique called optically stimulated luminescence (OSL) where there is no need of heating as readouts, annealing, etc. are done by optical meansusually at room temperature and emission of OSL is due to recombinations of electron-hole pairs released by optical stimulation [7]. Thus, stimulation is performed optically at room temperature and there is no need to heat the material, thereby avoiding the problem of thermal quenching. The commercially available TL dosimeters are LiF:Mg,Ti (TLD-100), LiF:Mg,Cu,P (TLD-700H), $CaSO_4$:Dy (TLD-900), CaF_2:Dy (TLD-200), Al_2O_3:C (TLD-500) [8]. It is, therefore, necessary to improve the TL/OSL characteristics of these phosphors or to develop some new ones.

Since last one decade many researchers have synthesized and studied a range of materials as OSL phosphors, such as, $NaLi_2PO_4$:Eu [5], MgO:Tb [9], $NaMgF_3:Eu^{2+}$ [10], $Y_3Al_5O_{12}$:C [11], Al_2O_3:B [12], $LiMgPO_4$:Tb, B [13], $LiAlO_2$ [14], $K_2Ca_2(SO_4)_3$:Cu [15], Na_2SiF_6:Cu,P [16], $NaLi_2PO_4:Ce^{3+}$ [17]. However, no phosphor could find sensitivity comparable to Al_2O_3:C (commercially available α-Al_2O_3:C of Landauer Inc.). The rare-earth (RE) doped $CaSO_4$ phosphor continuously receiving significant research interest due to their fundamental

characteristics and TL properties for applications in radiation dosimetry [18-27]. The high TL sensitivity of $CaSO_4$:RE phosphors makes them attractive candidates for use indosimetry [22]. Among them $CaSO_4$:Eu has been investigated mainly for radio-photoluminescence (RPL) dosimetry because of its demonstrated TL response to UV radiation in several orders of magnitude greater than that of other commonly known materials [28-33]. Previous studies have focused on the role of europium and the mechanism of TL in $CaSO_4$:Eu phosphor [28-33]. However, detail investigation of the effects of annealing temperatures on the TL and OSL response of $CaSO_4$:Eu phosphors not yet been established.

In the present report, $CaSO_4$:Eu in the nanocrystalline form have been synthesized by chemical method and studied its luminescence properties. $CaSO_4$:Eu have been annealed at different temperatures and its luminescence properties are investigated. The TL and OSL response of the $CaSO_4$:Eu nanophosphor have been investigated up to 100 Gy and theoretical fitting of the OSL decay, curve is done. First-principles Density Functional Theory (DFT) calculations have also been performed to gain atomistic insights into the luminescence properties of the pure $CaSO_4$ and $CaSO_4$:Eu materials, by predicting the electronic band structures and partial density of states (PDOS). They also show good correlations with the experimentally observed results.

2. Experimental

2.1. Synthesis of nanocrystalline and microcrystalline phosphor

Nanocrystalline $CaSO_4$:Eu phosphor was synthesized by chemical coprecipitation method considering the following chemical reaction [33, 34]. More details could be found in our earlier papers [33, 34],

$$(CH_3COO)_2Ca + (NH_4)_2SO_4 + EuCl_2(0.1\,mol\%) \xrightarrow{EtOH+H_2O} CaSO_4{:}Eu \downarrow + 2CH_3COONH_4 .$$

As prepared powder samples (dried at 150 °C) were further annealed and quenched at 400 °C to 1000 °C for 2 h in air. We have assigned $CaSO_4$:Eu@400, $CaSO_4$:Eu@500, etc. names to these samples for further analysis. Here, 400, 500, etc., indicate annealing temperatures in degree Celsius (°C). Microcrystalline samples were also prepared by the method suggested byYamashita et al. [22, 34]. For synthesis of $CaSO_4$:Eu (0.1 mol %) microcrystalline samples, the impurity doping was optimized 0.1 mol % using the $EuCl_2$. The powder obtained in the range

from 100 to 200 μm further annealed and quenched at 900 °C for 2 h. This sample named as Micro-$CaSO_4$:Eu@900 and used for further comparative studies.

2.2. Characterizations

To confirm the formation of the $CaSO_4$:Eu compound, X-ray diffraction pattern was studied at room temperature (Fig.1) by using Cu-target (Cu-K_α= 1.54 Å) on Bruker AXS D8 Advance X-ray Diffractometer (Bruker AXS, Inc.) and matching with the standard JCPDS data. X-ray diffraction analysis confirmed the formation of the $CaSO_4$:Eu compound and the phase transitions on annealing at different higher temperatures. The particle size and surface morphology of the samples was analyzed with Transmission Electron Microscope (TEM), TECHNAI G2 20U–TWIN (FEI, The Netherlands), operated at 200 kVand Scanning Electron Microscopy (SEM), JSM-6360A (JEOL–Japan) operated at 20 kV. Photoluminescence (PL) excitation and emission spectra were recorded using Horiba FluoroLog Spectrophotometer (Horiba Inc., Worldwide). TL, CW-OSL and thermally assisted OSL (TA-OSL) measurements were carried out using a Risø TL/OSL-DA-15 reader (Risø National Laboratory, Denmark) equipped with blue light-emitting diodes (LEDs) for stimulation (peak emission at 470 nm, ~ 30 mW/cm^2 at the sample position) and a bi-alkali photomultiplier tube (PMT) for light detection (9235QB, ET Enterprises Ltd., Uxbridge, UK). The heating rate for TL measurements were kept 5 $°Cs^{-1}$ and irradiations for the OSL and TL measurements were carried out using an inbuilt $^{90}Sr/^{90}Y$ beta source [15, 35]. The monochromatic OSL decay curves, for studying OSL spectra, were recorded on TL/OSL Research Reader, Model-1008, (Nucleonix, India) using a set of narrow-band (band width ±5 nm) filters (Edmund, USA).

2.3. Computational Details

The Vienna *Ab-initio* Simulation Package (VASP) was used for the density functional theory (DFT) calculations [36-38], a periodic plane wave DFT code which includes the interactions between the core and valence electrons using the Project Augmented Wave (PAW) method [39]. The electronic exchange–correlation potential was calculated using the Perdew–Burke–Ernzerhof (PBE) generalized gradient approximation (GGA) functional [40, 41]. A plane-wave basis set with a kinetic energy cutoff of 600 eV was tested to be sufficient to converge the total energy of the $CaSO_4$:Eu compound to within 10^{-6}eV and the residual Hellman–Feynman

forces in the ionic relaxations were converged to within 10^{-3}eV $Å^{-1}$. The Brillouin zone of $CaSO_4$ and $CaSO_4$:Eu supercells were sampled using 5×5×5 and 3×3×3 mesh of Monkhorst-Pack*k*-points, respectively [42]. The $CaSO_4$ was modelled in the hexagonal and orthorhombic phases with 2×2×2 supercells of the primitive unit cells such that the hexagonal phase contains 144 atoms (24 Ca, 24 S, and 96 O) and orthorhombic phase contains 192 atoms (32 Ca, 32 S, and 128 O).The replacement of one Ca atom with one Eu atom resulted in the formation of $CaSO_4$:Eu with compositions $Ca_{0.96}SO_4Eu_{0.04}$ and$Ca_{0.97}SO_4Eu_{0.03}$ for the hexagonal orthorhombic phases, respectively. A higherk-points mesh of 7×7×7was used to determine the electronic structures (band structure and partial density of states).

3. Results and discussion

3.1. Structural properties of $CaSO_4$:Eu

Fig. 1 shows the XRD spectra of $CaSO_4$:Eu nanophosphor, which confirms that the as-prepared $CaSO_4$:Eu sample is in hexagonal phase (JCPDS File No. 43-0606) [34, 43], while the sample annealed at 900 °C (i.e., $CaSO_4$:Eu@900) is in the orthorhombic phase (JCPDS Card No. 37-1496) [34]. The standard data of JCPDS File No. 43-0606 and 37-1496 also shown in the figure. The average grain size of the as-prepared phosphor (estimated using the Scherrer's formula) was found to be around ~15 nm [15]. The shape and size of these nanoparticles could also be seen in TEM/SEM images innanorod shape with 10-20 nm diameter and 200-300 nm length (Fig. 2a). It has also been found that they grow larger in size (2 to 4 μm) after annealing at around 900 °C (Fig. 2b). Above results supported by the XRD analysis, as the broadening of peaks of the annealed sample is reduced on annealing at higher temperature(s).

3.2. TL and OSL characterization

Fig. 3(a) shows the TL glow curves (heating rate = 5 $°Cs^{-1}$) and Fig. 3(b) shows the CW-OSL responseusing blue light (470 nm) stimulation for $CaSO_4$:Eu nanocrystalline samples annealed at different temperatures for an absorbed dose of 1 Gy from Sr^{90}/Y^{90} beta source. The TL glow curve has three peaks at 162, 225, 298 °C. A slight change in TL glow curve structure and shifting of the TL peaks are observed with increasing annealing temperature. This can be attributed to phase change and/or change in the particle size of $CaSO_4$:Eu on annealing up to

1000 °C as confirmed by XRD and SEM/TEM images [44]. Due to the change in the crystal structure, energy levels within the bandgap are reorganized and there may be a corresponding change in the glow peak temperatures. This could prominently be seen by comparing the difference in peak temperatures of $CaSO_4$:Eu@400 and $CaSO_4$:Eu@900 samples having TL peaks of the former at around 186, 241 and 301 ^oC while that of the later one at around 167, 225 and 297 ^oC, respectively. The changes in glow curve structures could also take place, however, it is not found that prominent as could be seen from TL glow curves of $CaSO_4$:Eu@600 and $CaSO_4$:Eu@900 samples (if we think that the particles have grown much bigger on annealing at 900 ^oC than at 600 ^oC for 2 h). The environment of the luminescent centers and hence glow curve structure could be affected by diffusion of atmospheric oxygen during annealing at much higher temperatures [45]. The doped impurity could also coexist in the host as Eu^{2+} or Eu^{3+}but their concentrations may change due to redox reactions on annealing at higher temperatures as well as on irradiations. For example, most of the Eu^{3+} impurity ions have been found to convert in to Eu^{2+} on annealing beyond 925 ^oC but not much conversion was observed on irradiation to γ-rays by Patil et al. [46] in their submicron particles. But conversion from Eu^{3+} to Eu^{2+} has mostly been observed on annealing at temperatures more than 800 ^oC. However, in our $CaSO_4$:Eu@900 sample we could also found Eu^{3+} to Eu^{2+} conversions (discussed below in Section 3.7). It would rather have more effect on the intensity(ies) than on the glow curve temperature as TL emission bands of these samples (annealed at different temperatures) would be in the different spectral ranges due to Eu^{2+} or Eu^{3+} ions concentrations (generated on annealing and irradiation) measuring different output intensities due to difference in spectral response of the optical detector (PMT) used for measuring TL output. The TL and OSL response with respect to the annealing temperature is shown in Fig. 3(c). The optimum TL and OSL response are obtained for the sample annealed at 900 °C, so further characterizations were mostly performed on $CaSO_4$:Eu@900.

3.3. Comparison of TL/OSL sensitivities

In Fig. 4 (a), we have provided comparative TL response and the Fig. 4 (b) shows the comparison of CW-OSL response of $CaSO_4$:Eu@900, microcrystalline $CaSO_4$:Eu@900 and commercially available α-Al_2O_3:Cphosphor powder (Landauer Inc.). The total TL intensity of the $CaSO_4$:Eu@900 is about $1/25^{th}$ times that of α-Al_2O_3:C and total TL intensity of Micro-$CaSO_4$:Eu@900 is about $1/140^{th}$ times that of α-Al_2O_3:C. The total OSL intensity of

$CaSO_4$:Eu@900 is about 1/29th times that of α-Al_2O_3:C and total OSL intensity of Micro-$CaSO_4$:Eu@900 is about 1/3484th times that of α-Al_2O_3:C. The comparison of TL and OSL sensitivities is as shown in Table 1.

3.4. TL and OSL response curves of $CaSO_4$:Eu@900

The TL and CW-OSL glow curves of the $CaSO_4$:Eu@900 exposed to Sr^{90}/Y^{90} beta source at the different doses from 0.02 Gy to 100 Gy are shown in Fig. 5(a) and Fig. 5(b), respectively. The Dose vs. TL (for 160 and 225 °C peak) and OSL response of $CaSO_4$:Eu@900 is shown in Fig. 5(c). The background is subtracted from the actual readings. A linear TL response is found in the range of 0.04 Gy to 100 Gy and the OSL response is linear from 0.02 Gy to 100 Gy.

3.5. Temperature dependence of OSL

The OSL intensity was investigated with respect to readout temperature using TA-OSL (Thermally Assisted-OSL) technique. In general, the OSL intensity increases with the stimulation temperatures and has been reported by various researchers. It was regarded due to the effect of readout temperature on the photo-ionization cross-section of OSL active traps. In this study, sample was optically stimulated with number of short pulses at low stimulation power. In this case TA-OSL intensity expressed by following equation [47-49]:

$$I_{TA-OSL} = Ae^{-\frac{E_A}{kT}} \quad (1)$$

where, A is a constant. The thermal assistance energy E_A can be calculated from the slope of the graph of ln($I_{TA\text{-}OSL}$) vs 1/kT. In the current studies, the short pulse duration was kept as 0.3 s after every 16 °C and TL taken simultaneously up to 330 °C (Fig. 6(a)) [50, 51]. The pulse height of the OSL signal vs. temperature was plotted in the Fig. 6(b). Fig. 6(c) shows the Arrhenius plot of ln($I_{TA\text{-}OSL}$) vs 1/kT. The activation energy was obtained at E_A= 0.0572 ± 0.0028 eV in theTA-OSL process.

3.6. Decay constant and photoionization cross-section

The CW-OSL decay curve fitted up to third order by the following equations [52]:

$$I_{CW-OSL} = A + I_1 \exp(-\sigma_1 \phi t) + I_2 \exp(-\sigma_2 \phi t) + I_3 \exp(-\sigma_3 \phi t) \quad (2)$$

$$I_{CW-OSL} = A + I_1 \exp\left(-\frac{t}{\tau_1}\right) + I_2 \exp\left(-\frac{t}{\tau_2}\right) + I_3 \exp\left(-\frac{t}{\tau_3}\right) \quad (3)$$

where,$\sigma = \frac{1}{\phi\tau}$, I_{CW-OSL} is the OSL intensity, I_1, I_2 and I_3 are the initial intensities of the fast, medium, and slow decay components of CW-OSL curve, σ_1, σ_2 and σ_3 is the photoionization cross-sections; τ_1, τ_2 and τ_3 are the decay constants, and ϕ is stimulating photon intensity (photons/cm^2/s). Fig. 7 shows the experimentally obtained CW-OSL curve (in black) and theoretically fitted exponential decay curve (in pink) for $CaSO_4$:Eu@900 sample (exposed to 1 Gy dose from Sr^{90}/Y^{90} beta source). The three components are shown in blue, green and light blue. The variation of (Expt.-Fit)/Fit with time is shown in the inset. The experimental data very well matches with the fitted curves. The values of σ and τ for all three OSL traps are shown in Table 2.

3.7. PL and OSL spectra

Typical PL excitation for $CaSO_4$:Eu (for emissions at wavelengths 385 nm and 616 nm for Eu^{2+} and Eu^{3+}, respectively) and emission spectra by exciting with 320 nm and 253 nm the sample again for Eu^{2+} and Eu^{3+}, respectively) is shown in Fig. 8. There are several peaks at around 277, 320, 337, 349 are seen in the excitation spectra of Eu^{2+} for emission at 385 nm (Fig. 8, curve b). These excitation bands arise from the transition from $^8S_{7/2}$ state of $4f^7$ configuration to the states belonging to $4f^65d^1$ configuration. Eu^{2+} emission is in form of a narrow band around 385 nm. This emission arises from the lowest band of $4f^65d^1$ configuration to $^8S_{7/2}$ state of $4f^7$ configuration. On excitation by 320 nm, only one prominent peak around 385 nm was observed in emission spectra of Eu^{2+}(Fig. 8, curve c). It was difficult to observe very distinct peaks in the excitation spectrum of Eu^{3+} (Fig. 8, curve a) as 308 nm band (the second order of the emission 616 nm) mixes with the spectrum. However, a shoulder around 253 and 277 nm could be seen. The material, therefore, was excited by 253 nm to record the emission spectrum of Eu^{3+} and several emission peaks were observed at around 570, 593, 616, 696, and 700 nm in this spectrum (Fig. 8, curve d). These bands are corresponding to transitions $^5D_0 \rightarrow {}^7F_0$, $^7F_1$, $^7F_2$, $^7F_3$, $^7F_4$ levels of Eu^{3+}, respectively. The f–f transitions of Eu^{3+}, on the other hand, are forbidden and Eu^{3+} PL is in general weak, unless there is excitation by charge transfer or energy transfer from a sensitizer. Exact positions, fine structure and relative intensities of these bands also depend on the local environment of Eu^{3+} ion. In $CaSO_4$, incorporation of Eu^{3+} must be accompanied by charge compensation. Charge compensation and hence the local environment of Eu^{3+} ion can depend on the method of preparation, heat treatments and irradiation, etc. Excitation around 253 nm is

corresponding to CT band of Eu^{3+}.

The effect of annealing on the Eu^{2+}/Eu^{3+} concentrations could be seen in emission spectra of the samples annealed at different high-temperatures (in the range of 400 -1000 ^{o}C). The emission spectra excited by 320 nm wavelength are shown in Fig. 9. It could be clearly seen that the intensity of the 385 nm peak corresponding to Eu^{2+} increases till 800 ^{o}C and decreases thereafter, on the contrary, the emission spectra (excited by 253 nm wavelength) of the Eu^{3+} found to show the reverse trend as shown in Fig. 9 (inset). Above 800 ^{o}C, the unusual results may be due to decomposition of $CaSO_4$ to CaS or due to diffusion of atmospheric oxygen in the matrix. It may also be attributed to change in the Eu^{3+} environment due to phase change from hexagonal to orthorhombic phase around this temperature.

The effect of radiation on the concentration of Eu^{2+}/Eu^{3+} could also be seen in the emission spectra of the $CaSO_4$:Eu@900. The emission spectra of unirradiated and irradiated (1 kGy of gamma-rays from ^{60}Co radioactive source) sample corresponding to Eu^{2+} is as shown in Fig. 10. The same for Eu^{3+} is also seen in Fig. 10 (inset). The increase in the peak intensity for Eu^{2+} emission peak and the decrease in Eu^{3+} on irradiation could be seen. These results show that redox reactions take place during annealing as well as on irradiation. Such results were observed for other samples also but not given here due to paucity of the space.

The OSL spectra of the$CaSO_4$:Eu@900 phosphor material was tried on the Nucleonix (India) OSL/TL Research Reader (Model TL/OSL 1008) attached with an optical fiber and CCD (Linear Silicon CCD array detector type SONY ILX511B 2048 PI) based spectrophotometer (Ocean Optics, Model 2000+). However, due to less sensitivity of the CCD and fast decay of the OSL, it was not possible to take good OSL spectra. Therefore, a set of very narrow band ($\pm$5 nm bandwidth) interreference filters was used to record monochromatic OSL decay curves for different wavelengths and the maximum intensity of the curves was plotted with wavelengths. A typical OSL spectrum of the $CaSO_4$:Eu@900 sample stimulated by blue LED light (~470 nm, ~30 mW/cm^2 at the sample position) is as shown in Fig. 11. The material was irradiated to 10 Gy from ^{90}Sr/^{90}Y beta source. The OSL decay curves taken with the filters of different wavelengths are also shown in the inset.

It could be seen in the figure that there are two prominent peaks (bands) appear one around 320 nm and another 385 nm. The small band around 470 nm may be due to little intensity of LED light after using the Schott GG-420 filter. The OSL emission bands may be attributed to $^5P_{7/2} \rightarrow {}^8S_{7/2}$ Eu^{2+} transitions and are almost similar to the ones observed in photoluminescence

(PL) studies. These results are also similar to the results already available in the literature [46, 53]. As reported earlier [28, 45, 54], in $CaSO_4$:Eu, Eu exists in the divalent as well as the trivalent state in the $CaSO_4$ lattice and emits fluorescence on both the valency states. The redox reactions in Eu doped $CaSO_4$ phosphor, i.e., conversion of $Eu^{3+} \leftrightarrow E^{2+}$ on annealing as well as on irradiation are well known [53]. It may be presumed that during the beta-rays irradiation electron-hole pairs are generated; the electrons are trapped by anion vacancies and the holes by Eu^{2+}, forming F-centers and Eu^{3+} ions, while part of the F electrons may recombine radiatively with Eu^{3+}. Therefore, it can be interpreted that Eu^{3+} ions are transformed to Eu^{2+} ions during high-temperature treatment in air, and Eu^{2+} ions are more stable than Eu^{3+} ions in $CaSO_4$:Eu material. However, at very high-temperature (more than 800 ^oC), $CaSO_4$ is known to decompose to CaS [53]. Also, there are some reports that the atmospheric oxygen also may get diffused/incorporated inside the materials and make certain changes and/or stop further decomposition. Such changes may change the concentration of Eu^{2+}/Eu^{3+} due to charge compensation [53]. This has been clearly seen in the PL emission spectra of the material annealed at different temperatures (Fig. 9). It could also be seen that the concentration of Eu^{2+} ions (385 nm emission band on excitation by 320 nm) is low for the sample annealed at 400 ^oC (i.e., $CaSO_4$:Eu@400 sample) and increases with the annealing temperature till 800 ^oC and decreases on annealing at further higher temperatures. It could also be seen that the intensity of 385 nm peak increases on irradiation (Fig. 10) for the $CaSO_4$:Eu@900 sample. This indicates that there is more conversion $Eu^{3+} \rightarrow Eu^{2+}$ and Eu^{2+} could be more stable than Eu^{3+}. It could also be seen that it is not only the doping concentration or its initial oxidation state in $CaSO_4$:Eu phosphor that changes its sensitivity but also the temperature at which it has been annealed may change its sensitivity due to changes in its crystal structure, morphology, redox reactions, etc. [53, 55, 56]. As reported by Tang, et al. [57, 58], TL emission spectra of $CaSO_4$:Eu not only consists of emission peaks at 385 nm, which comes from transitions between energy levels of Eu^{2+} but also peaks at around 590, 620 and 700 nm indicating that TL emission also comes also comes from the transitions between the energy levels of Eu^{3+} for the samples annealed at different temperatures. They, however, have observed that only 385 nm peak in their OSL emission spectra which again could be attributed to Eu^{2+} states. We also observed the OSL emission due to Eu^{2+} (385 nm) in our $CaSO_4$:Eu@900 sample. This indicates that though the kinds of luminescence centers and traps generated on irradiation may be the same but all the traps/luminescence centers might not be taking part in OSL process (contrary to the TL

processes, where all kinds of traps/luminescence centers are involved) and would depend on the stimulation wavelength (energy) that which kind of traps/luminescence centers would be stimulated. In our sample it was found that the traps/luminescence centers related to Eu^{2+} are only taking part in the process.

3.8. Electronic structures

In order to gain an atomistic insight into the luminescence properties of the $CaSO_4$ and $CaSO_4$:Eu materials, we have studied electronic properties using Density Functional Theory on the geometry optimized structures of the pure $CaSO_4$ and doped $CaSO_4$:Eu materials considering both the hexagonal and orthorhombic phases. A 2×2×2 supercell of the hexagonal (containing 144 atoms (24 Ca, 24 S, and 96 O)) (Fig. 12 a and d) and orthorhombic (containing 192 atoms (32 Ca, 32 S, and 128 O)) (Fig. 13 a and d) crystal structures of $CaSO_4$ was employed to model $CaSO_4$:Eu, where one Ca atom was replaced with one Eu atom giving the compositions $Ca_{0.96}SO_4Eu_{0.04}$ and $Ca_{0.97}SO_4Eu_{0.03}$, respectively. The fully optimized lattice parameters for the 2×2×2 supercell of hexagonal $CaSO_4$ are predicted at a= 14.076 Å and c=12.702 Å, compared to a= 14.123 Å and c=12.810 Å for $CaSO_4$:Eu. For the orthorhombic phase, the optimized lattice parameters for the 2×2×2 supercell are predicted at a = 14.065 Å and c = 12.506 Å, compared to a = 14.100 Å and c = 12.5144 Å. The results indicate that Eu doping induces small expansion in the lattice, which is consistent with the larger ionic radius of Eu^{2+} (1.31 Å) than Ca^{2+} (1.14 Å). The electronic band structures and projected density of states for the hexagonal and orthorhombic models of $CaSO_4$ and $CaSO_4$:Eu are shown in Fig. 12 and 13, respectively. An analysis of the band structure of both phases of pure $CaSO_4$ revealed that both the conduction band minimum (CBM) and valence band maximum (VBM) are located at Γ high-symmetry point in the Brillouin zone, making $CaSO_4$ a direct band gap insulator with predicted band gap of 5.67 eV for the hexagonal phase and 5.86 eV for the orthorhombic phase. Compared to the pure $CaSO_4$, we observe the introduction of donor states in the bandgap near Fermi level and the valence band edge of Eu-doped $CaSO_4$:Eu. Also, both the VBM and CBM shift to lower energy levels but the band gaps are essentially preserved. Through the intermediate (donor) states in the band gap, electrons in the valence band maxima can be excited by the low energy photons to the conduction band minima, which could result in enhanced carrier concentration in $CaSO_4$:Eu. The total and partial density of states (PDOS) of $CaSO_4$ and $CaSO_4$:Eu reveal that the top of the valence band is mainly composed of O-*p* orbitals in $CaSO_4$, whereas in $CaSO_4$:Eu, there is an

additional contribution from Eu-*d* orbitals to the O-*p* orbital to the VBM. The bottom of the conduction band is mainly composed of Ca-*d* orbitals.These results provide atomistic insights into the luminescence behavior (especially, changes in glow curve structures and their relative intensities) of $CaSO_4$ and $CaSO_4$:Eu, which can mainly be attributed to the charge intransitions near the absorption edge from O-*p*→Ca-*d* orbitals in $CaSO_4$ and through O-*p*→Eu-*d*→Ca-*d* orbitals in $CaSO_4$:Eu.

4. Conclusion

The facile chemical method used for synthesis of $CaSO_4$:Eu nanophosphor. The morphology of as-synthesized $CaSO_4$:Eu shows nanorod shape with a diameter of ~15 nm and the length of ~250 nm. At 900 °C annealed $CaSO_4$:Eu observed phase transformation from hexagonal to orthorhombic with significant improved particle size. Obvious differences were observed in the TL glow curve structure with increasing annealing temperatures, with the maximum TL and OSL sensitivity obtained at 900 °C. The $CaSO_4$:Eu phosphor annealed at 900 ^oC exhibits a linear TL and OSL response in the range from 0.04 Gy to 100 Gy and 0.02 Gy to 100 Gy respectively. The activation energy (E_A) for the TA-OSL process was found to be 0.0572 ± 0.0028 eV. The experimentally obtained CW-OSL curve was theoretically fitted into three components having photoionization cross-sections of 5.56×10^{-17}, 4.02×10^{-18} and 1.37×10^{-18} respectively. The results on PL and OSL spectra suggest that both ionic states of the impurity (Eu^{2+} and Eu^{3+}) exist in the $CaSO_4$:Eu phosphor. However, redox reactions take place on annealing and irradiation. But Eu^{2+} state seems to be more stable and the OSL emission comes mostly from the energy levels of this state unlike in TL process where emission could be attributed to both the ionic states of the impurity. DFT calculation was used to analyze the crystal structures and electronic structures of hexagonal and orthorhombic $CaSO_4$ and $CaSO_4$:Eu, showing that both materials are direct bandgap (5.67−5.86 eV) insulators, with Ca^{2+} substitution by Eu^{2+} found to introduce donor states in the bandgap near Fermi level and the valence band edge of $CaSO_4$:Eu. These results are useful in understanding the luminescence behavior of these materials, which can be attributed mainly to the charge transitions near the absorption edge from O-*p*→Ca-*d* orbitals in $CaSO_4$ and through O-*p*→Eu-*d*→Ca-*d* orbitals in $CaSO_4$:Eu.

Acknowledgements

Nandkumar T. Mandlik (NTM) gratefully acknowledges the Department of Science and Technology (DST) for providing funds under DST-FIST program, the Savitribai Phule Pune University (SPPU), Pune for partial financial assistance under the University Research Grant Scheme (Project No. 14SCI000402), University Grants Commission (UGC), New Delhi for providing funds under "College of Excellence" (CE) scheme and Department of Biotechnology (DBT), New Delhi for providing financial assistance under "DBT-STAR College" scheme. One of the authors (NYD) also acknowledges the UK Engineering and Physical Sciences Research Council (EPSRC) for funding (Grant No. EP/S001395/1). This work has also used the computational facilities of the Advanced Research Computing at Cardiff (ARCCA) Division, Cardiff University and HPC Wales. We also acknowledge the use of the facilities of ARCHER (http://www.archer.ac.uk), the UK's national supercomputing service via our membership of the UK's HEC Materials Chemistry Consortium, which isfunded by EPSRC (EP/L000202). P. D. Sahare (PDS) would also like to acknowledge the partial financial assistance by Inter-University Accelerator Center, New Delhi through the BTR-3 research project code No. 64325. We also acknowledges Dr. Munish Kumr, Scientist, Bhabha Atomic Research Center (BARC), Mumbai for providing TL/OSL measurements.

References:

[1] International Topical Meeting on Nuclear Research Applications and Utilization of Accelerators, 4–8 May 2009 Vienna, Austria.

[2] S. W. S. McKeever, Thermoluminescence of Solids, Cambridge University Press, (1985).

[3] S. W. S. McKeever, M. Moscovitch, P. D. Townsend, Thermoluminescence Dosimetry Materials: Properties and Uses. Nuclear Technology Publishing, Ashford, UK, (1995).

[4] V. Kortov, Radiat. Meas. 42 (2007) 576-581.

[5] P. D. Sahare, Manveer Singh, Pratik Kumar, RSC Adv. 5 (2015) 3474–3481.

[6] A. J. J. Bos, Radiat. Meas. 41 (2007) S45– S56.

[7] E. G. Yukihara, G. O. Sawakuchi, S. Guduru, S. W. S. McKeever, R. Gaza, E. R. Benton, N. Yasuda, Y. Uchihori, H. Kitamura, Radiat. Meas. 41 (2006) 1126-1135.

[8] Numan Salah, Zishan H. Khan, Sami S. Habib, Nucl. Instr. Meth. Phys. Res. B 269 (2011) 401–404.

[9] A. J. J. Bos, M. Prokic, J. C. Brouwer, Radiat. Prot. Dosim. 119 (2006) 130-133.

[10] C. Dotzler, G. V. M. Williams, U. Rieser, A. Edgar, Appl. Phys. Lett. 91 (2007) 121910, 1-3.

[11] M. S. Kulkarni, K. P. Muthe, N. S. Rawat, D. R. Mishra, M. B. Kakade, S. Ramanathan, S. K. Gupta, B. C. Bhatt, J. V. Yakhmi, D. N. Sharma, Radiat. Meas. 43 (2008) 492-496.

[12] A. Soni, K. P. Muthe, M. S. Kulkarni, D. R. Mishra, B. C. Bhatt, S. K. Gupta, J. V. Yakhmi, D. N. Sharma, J. Lumin. 130 (2010) 1308-1312.

[13] B. Dhabekar, S. N. Menon, E. Alagu Raja, A. K. Bakshi, A. K. Singh, M. P. Chougaonkar, Y. S. Mayya, Nucl. Instr. Meth. Phys. Res. B 269 (2011) 1844-1848.

[14] J. I. Lee, A. S. Pradhan, J. L. Kim, I. Chang, B. H. Kim, K. S. Chung, Radiat. Meas. 47 (2012) 837-840.

[15] Nandkumar Mandlik, P. D. Sahare, M. S. Kulkarni, B. C. Bhatt, V. N. Bhoraskar, S. D. Dhole, J. Lumin. 146 (2014) 128-132.

[16] R. A. Barve, R. R. Patil, S. V. Moharil, N. P. Gaikwad, B. C. Bhatt, R. Pradeep, D. R. Mishra, M. S. Kulkarni, Radiat. Prot. Dosim. 163 (2015) 439-445.

[17] P. D. Sahare, Neyaz Ali, N. S. Rawat, Shaila Bahl, Pratik Kumar, J. of Lumin. 174 (2016) 22–28.

[18] K. Shinsho, E. Watanabe, A. Urushiyama, J. Appl. Phys. 100 (2006) 093514, 1–6.

[19] A. R. Lakshmanan, Prog. Mat. Sci. 44 (1999) 1–187.

[20] A. R. Lakshmanan, Phys. Status Solidi (a) 186 (2001) 153–166.

[21] A. R. Lakshmanan, S. B. Kim, B. G. Kum, H. M. Jang, B. C. Kang, Phys. Status Solidi (a) 203 (2006), 565–577.

[22] T. Yamashita, N. Nada, H. Onishi, S. Kitamura, Health Phys. 21 (1971) 295–300.

[23] R. L. Calvert, R. J. Danby, Phys. Status Solidi, 83 (1984) 597–604.

[24] X. Gong, L. Liu, W. Chen, J. Appl. Phys. 88 (2000) 4389–4393.

[25] X. Gong, P. Wu, W. K. Chan, W. Chen, J. Phys. Chem. Solids 61 (2000) 115–121.

[26] X. Gong, P. Wu, W. K. Chan, W. Chen, Opt. Mater. 15 (2000) 143–148.

[27] N. B. Ingle, S. K. Omanwar, P. L. Muthal, S. M. Dhopte, V. K. Kondawar, T. K. Gundurao, S. V. Moharil, Radiat. Meas. 43 (2008) 1191-1197.

[28] S. M. Dhopte, P. L. Muthal, V. K. Kondawar, S. V. Moharil, J. of Lumin. 50 (1991) 187-195.

[29] J. Azorin, C. Furetta, A. Scacco, Phys. Stat. Sol. (a) 138 (1993) 9–43.

[30] S. V. Upadeo, T. K. Gundurao, S. V. Moharil, J. Phys.:Condens. Matter 6 (1994) 9459-9468.

[31] S. R. Nair, V. K. Kondawar, S. V. Upadeo, S. V. Moharil, T. K. Gundurao, J. Phys.: Condens. Matter 9 (1997) 8307–8323.

[32] M. S. Kulkarni, R. R. Patil, A. Patle, N. S. Rawat, P. Ratna, B. C. Bhatt, S. V. Moharil, Radiat. Meas.71 (2014) 95-98.

[33] Nandkumar Mandlik, V. N. Bhoraskar, B. J. Patil, S. S. Dahiwale, P. D. Sahare, S. D. Dhole, Indian J. of Pure and Appl. Phy. 55 (2017) 413-419.

[34] Nandkumar Mandlik, S. D. Dhole, P. D. Sahare, J. S. Bakare, A. Balraj, B. C. Bhatt, App. Radiat. Isotop. 148 (2019) 253–261.

[35] E. G. Yukihara, Radiat. Meas. 46 (2011) 580-587.

[36] G. Kresse, D. Joubert, Phys. Rev. B. **59,** (3) (1999) 1758-1775.

[37] G. Kresse, J. Furthmüller, Comput. Mater.Sci., **6,** (1996) 15-50.

[38] G. Kresse, J. Hafner, Phys. Rev. B: Condens. Matter Mater. Phys. 47 (1993) 558–561.

[39] P. E. Blöchl, Phys. Rev. B: Condens. Matter Mater. Phys. 50 (1994) 17953-17979.

[40] J. P. Perdew, K. Burke, M. Ernzerhof, Phys. Rev. Lett., 78 (1997) 1396.

[41] J. P. Perdew, K. Burke, M. Ernzerhof, Phys. Rev. Lett. 77 (1996) 3865–3868.

[42] H. J. Monkhorst, J. D. Pack, Phys. Rev. B: Solid State 13 (1976) 5188.

[43] Aarti Muley, R. R. Patil, S. V. Moharil, Ce^{3+}emission in hexagonal and orthorhombic phases of $CaSO_4$, J. Lumin. 128 (2008) 509-512.

[44] A. K. Bakshi, A. S. Pradhan, A. K. Tyagi, R. K. Kher, B. C. Bhatt, Radiat. Prot. Dosim. 119 (2006) 139–142.

[45] A. K.Bakshi, S. J. Patwe, M. K. Bhide, B. Sanyal, V. Natarajan, A. K. Tyagi, R. K. Kher, J. Phys. D: Appl. Phys. 41 (2008) 25402, 1-8.

[46] R. R. Patil, P. L. Muthal, S. M. Dhopte, V. K. Kondawar, S. V. Moharil, J. Lum. 126 (2007) 571–574.

[47] D. R. Mishra, Anuj Soni, N. S. Rawat, M. S. Kulkarni, B. C. Bhatt, D. N. Sharma, Radiat. Meas. 46 (2011) 635-642.

[48] A. Soni, D. R. Mishra, B. C. Bhatt, S. K. Gupta, N. S. Rawat, M. S. Kulkarni, D. N. Sharma, Radiat. Meas. 47 (2012) 111-120.

[49] B. C. Bhatt, Anuj Soni, G. S. Polymeris, D. K. Koul, D. K. Patel, S. K. Gupta, D. R. Mishra, M. S. Kulkarni, Radiat. Meas. 64 (2014) 35-43.

[50] G. A. T. Duller, A. G. Wintle, Nucl. Tracks, Radiat. Meas. 18 (1991) 379-384.

[51] G. A. T. Duller, L. Botter-Jenson, Radiat. Prot. Dosim. 47 (1993) 683-688.

[52] N. S. Rawat, M. S. Kulkarni, M. Tyagi, P. Ratna, D. R. Mishra, S. G. Singh, B. Tiwari, A. Soni, S. C. Gadkari, S. K. Gupta, J. Lum. 132 (2012) 1969–1975.

[53] A. M. Muke, P. L. Muthal, S. M. Dhopte, S. V. Moharil, J. Lum. 132 (2012) 342–344.

[54] V. N. Bapat, Solid State Phys.,10 (1977) L465 -L467.

[55] P. D. Sahare, J. S. Bakare, S. D. Dhole, N. B. Ingale, A. A. Rupasov, J. Lum. 130 (2010) 258-265.

[56] G. Rani, P. D. Sahare, NIM B 311 (2013) 71-77.

[57] D. L. Luo, Q. Tang, J. Y. Guo, C. X. Zhang, Acta Physica Sinica, 64, (2015) 087805-5.

[58] Q. Tang, C. Zhang, Nucl. Techn. 28 (2005) 375-378.

Figure Captions:

Fig. 1. X-ray diffraction pattern of $CaSO_4$:Eu nanophosphor (a) as–prepared with hexagonal phase, (b) annealed at 900 °C with orthorhombic phase. The standard data of JCPDS File No. 43-0606 and 37-1496 also shown in the figure.

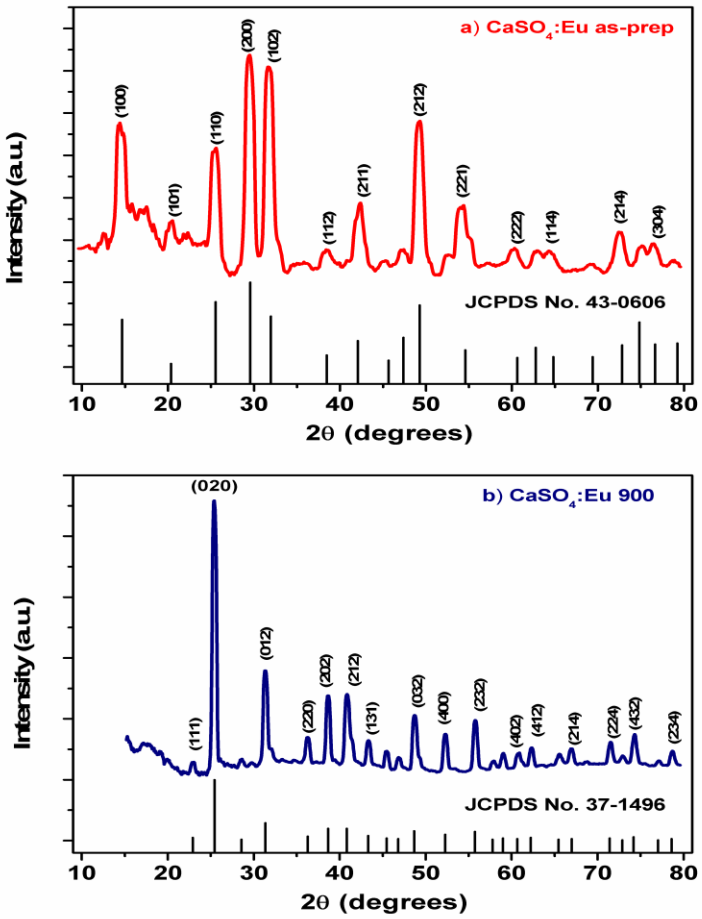

Fig. 2. a) TEM image of as prepared $CaSO_4$:Eu nanophosphor, **b)** SEM image of $CaSO_4$:Eu nanophosphor annealed at 900 °C.

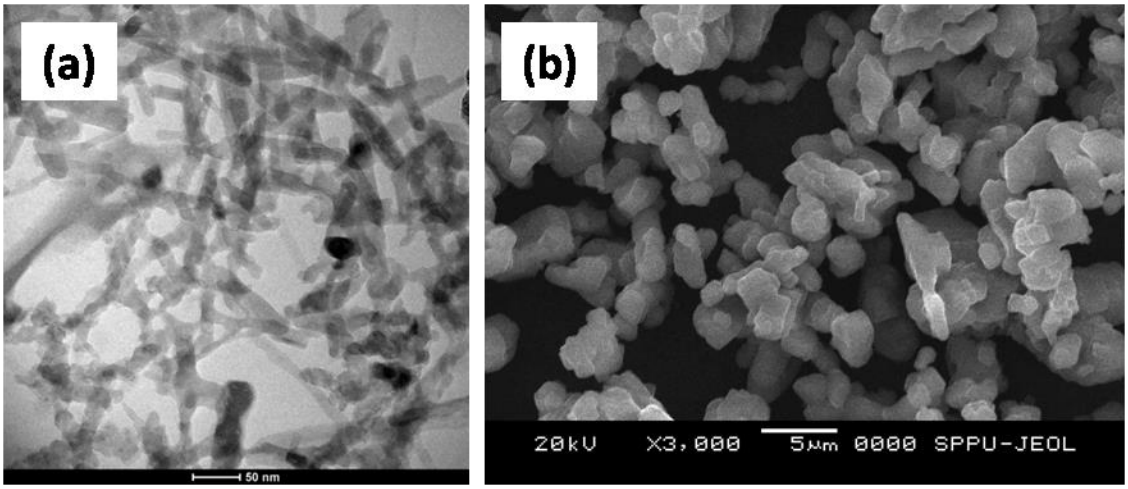

Fig. 3. (a) TL glow curves and **(b)** CW-OSL curves of $CaSO_4$:Eu nanophosphor annealed for 2 h at different temperatures (400 °C to 1000 °C) for an absorbed dose of 1 Gy from Sr^{90}/Y^{90} beta source. **(c)** Effect of annealing temperature on the (i) TL response (ii) CW-OSL response of the $CaSO_4$:Eu phosphor.

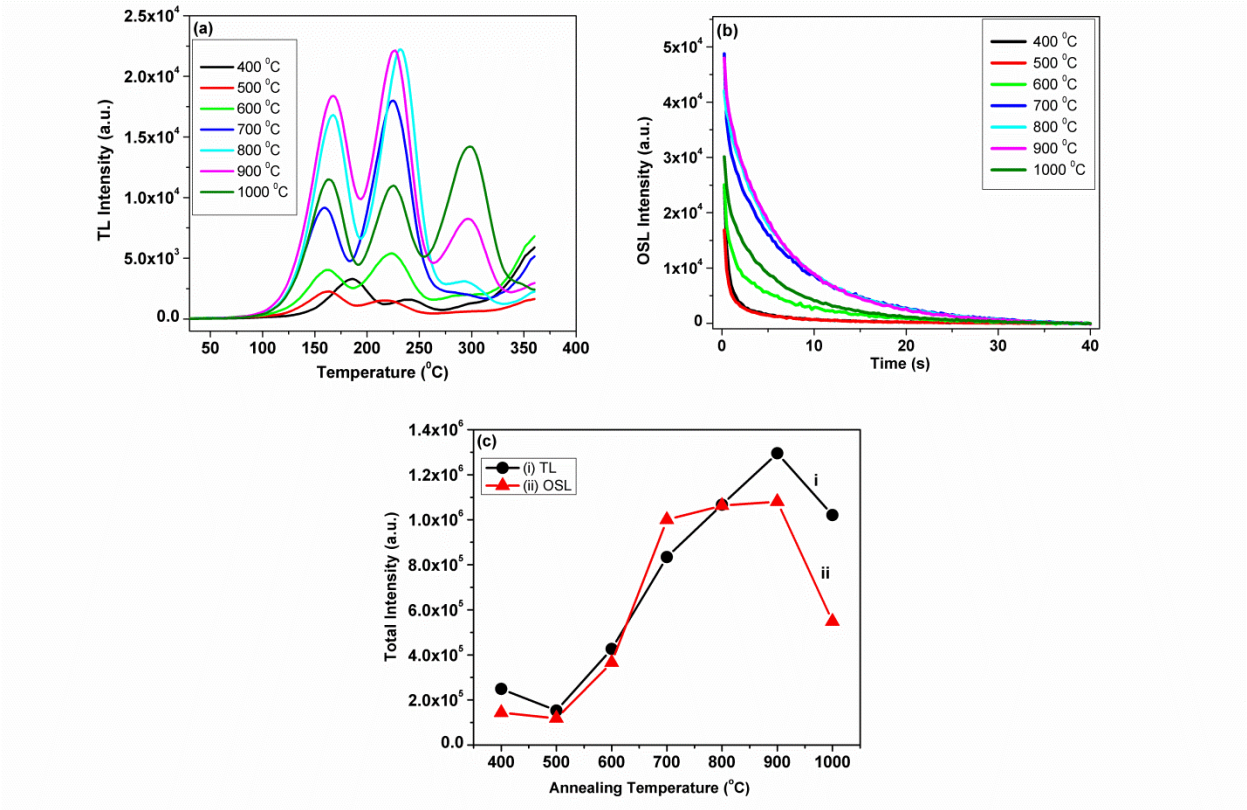

Fig. 4. (a) TL glow curves and **(b)** CW-OSL curves of various phosphors exposed to 1 Gy from Sr^{90}/Y^{90} beta source. (a) Microcrystalline $CaSO_4$:Eu@900, (b) $CaSO_4$:Eu@900, (c) Commercial α-Al_2O_3:C. The ordinate is to be multiplied by the numbers at the curves to get the relative intensities.

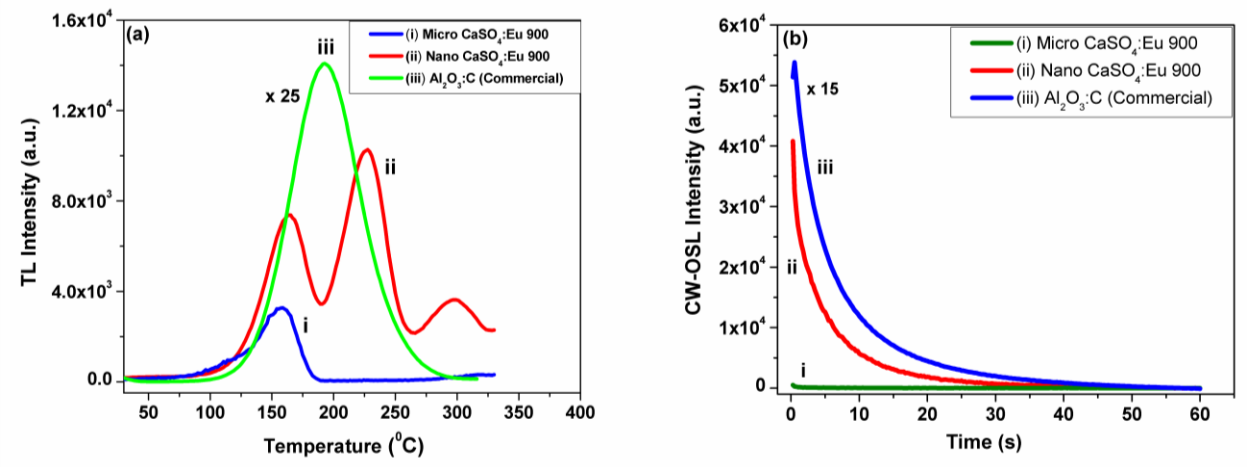

Fig. 5 (a) TL glow curves and **(b)** CW-OSL curves of $CaSO_4$:Eu@900 phosphor. **(c)** Dose vs. TL and OSL response of $CaSO_4$:Eu@900 phosphor **(i)** TL response of 160 °C peak (slope of fitted line = 0.94) **(ii)** TL response of 225 °C peak (slope of fitted line = 0.94) **(iii)** OSL response (total OSL intensity vs. dose) (slope of fitted line = 0.985). $CaSO_4$:Eu@900 phosphor exposed to Sr^{90}/Y^{90} beta source at the different doses from 0.02 Gy to 100 Gy. The correlation coefficient (R^2) of the linear fits for all curves is found to be 0.999.

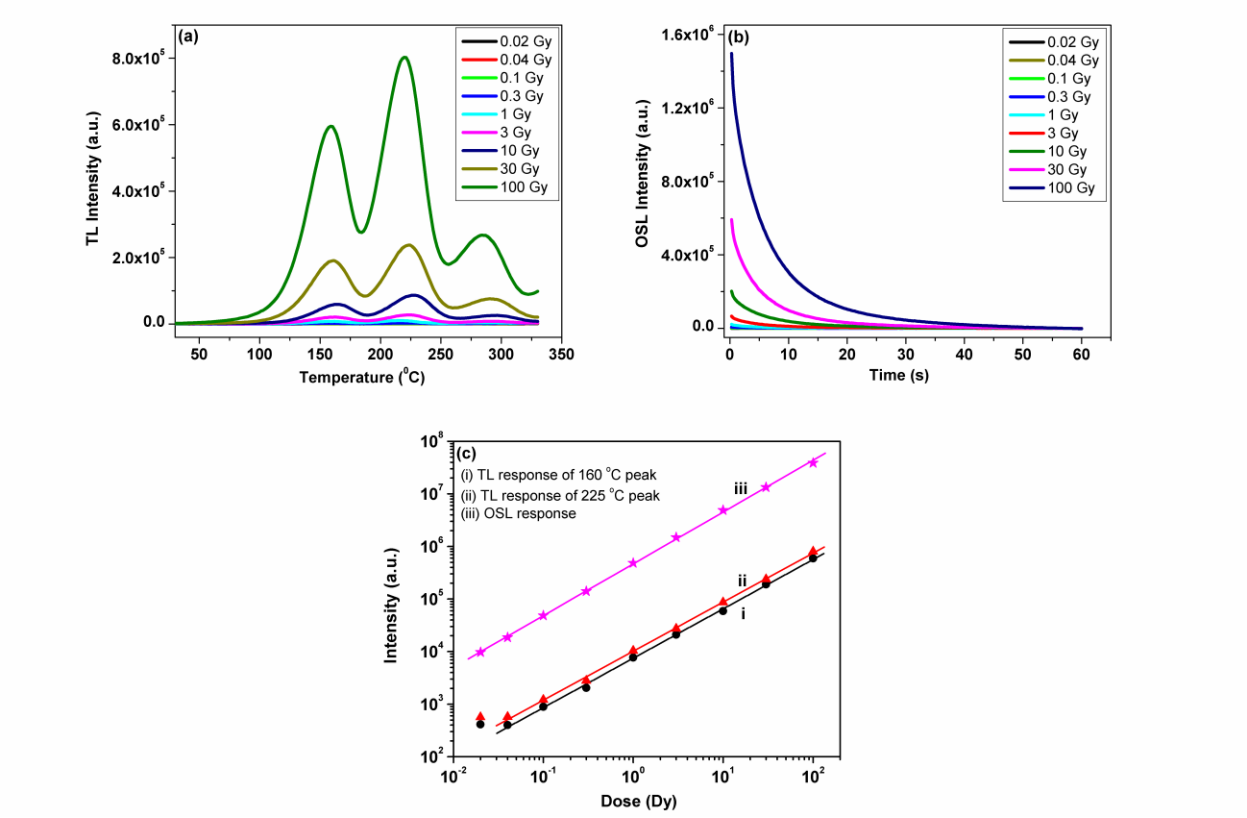

Fig. 6 (a) Thermo-Optical Luminescence (TOL) measurements of $CaSO_4$:Eu@900 phosphor obtained with short (0.3 s) and low power illumination (90 % LED power) (for every 16 ^oC when heating at 5 $°Cs^{-1}$) of a sample previously irradiated to 1 Gy. **(b)** TA-OSL signal, i.e., the pulse height of Fig. 6(a) vs temperature. **(c)** Arrhenius analysis of the integrated TA-OSL signal from Fig. 6(b). The straight-line fit yields the activation energy for the thermally assisted OSL (TA-OSL) process $E_A = 0.0572 \pm 0.0028$ eV.

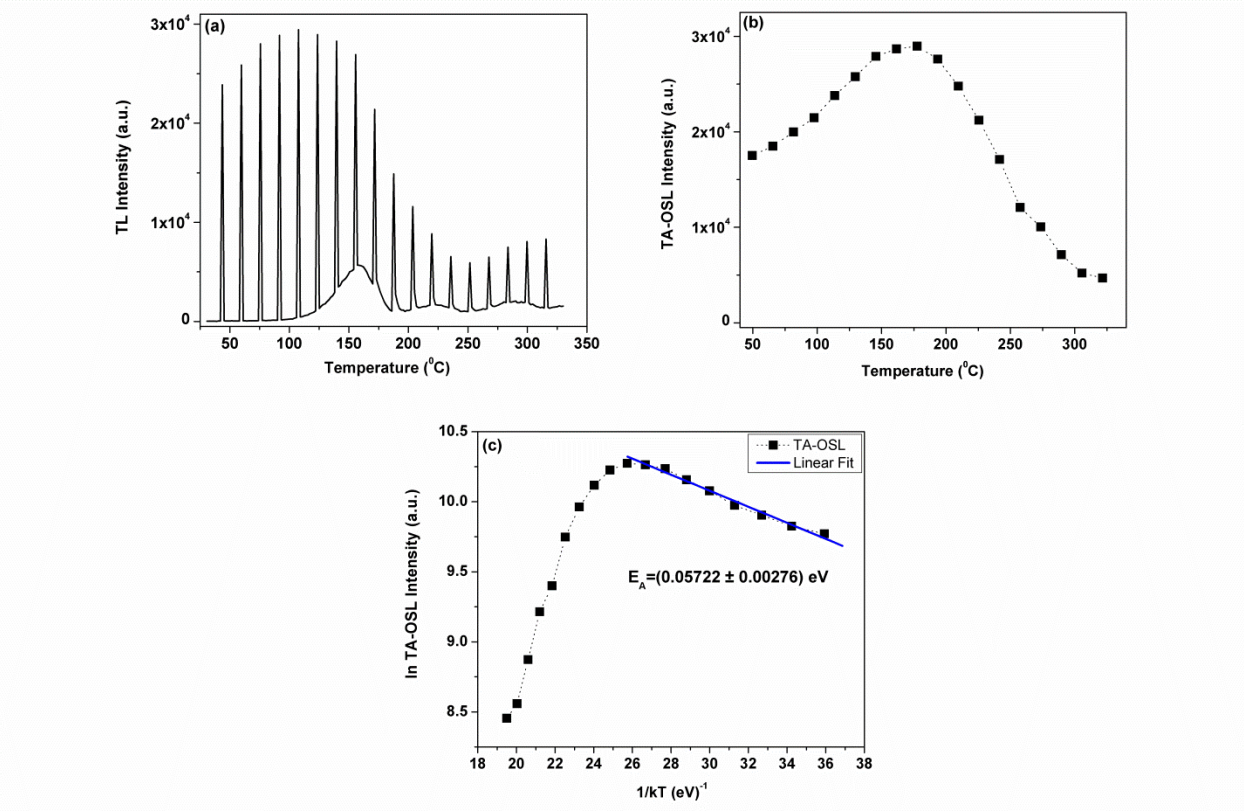

Fig.7. The experimentally obtained CW-OSL curve (in black) and theoretically fitted exponential decay curve (in pink) for $CaSO_4$:Eu@900 phosphor (exposed to 1 Gy dose from Sr^{90}/Y^{90} beta source). The three components are shown in blue, green and light blue. The variation of (Expt.-Fit)/Fit with time is shown in the inset.

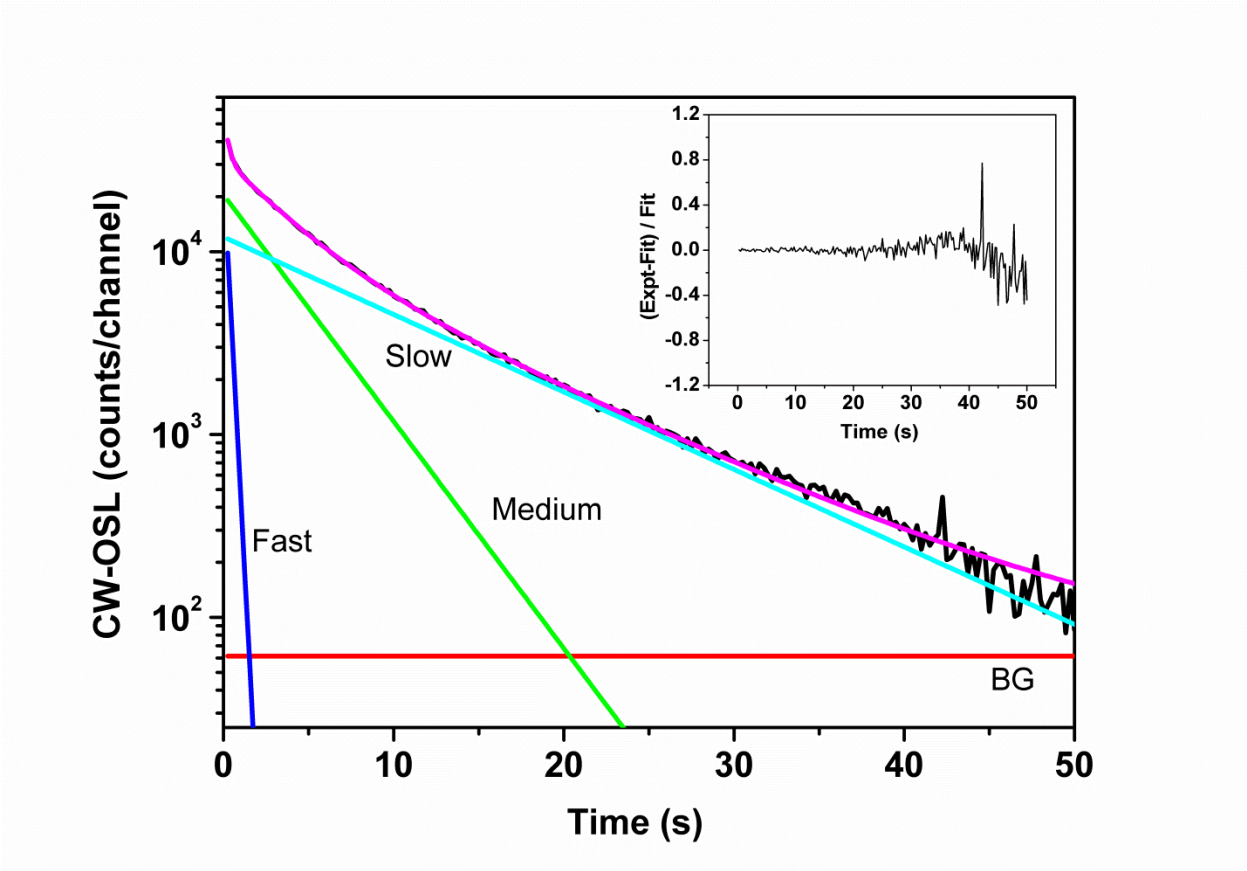

Fig. 8. Photoluminescence excitation and emission spectra of $CaSO_4$:Eu@700 phosphor. **(a)** Excitation spectrum for emission at 616 nm (curve a), **(b)** Excitation spectrum for emission at 385 nm (curve b), **(c)** Emission spectrum excited by 320 nm wavelength (curve c), **(d)** Emission spectrum excited by 253 nm wavelength (curve d).

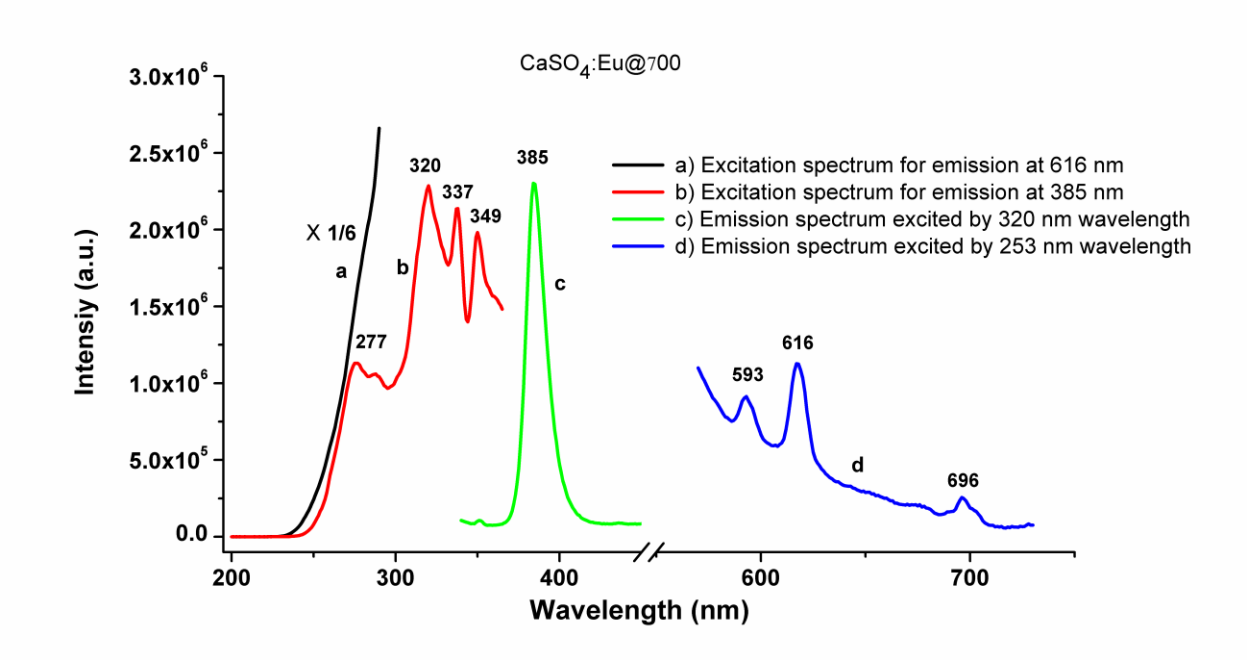

Fig. 9. Photoluminescence emission spectra of $CaSO_4$:Eu phosphors (excited by 320 nm wavelength) annealed at different temperatures.

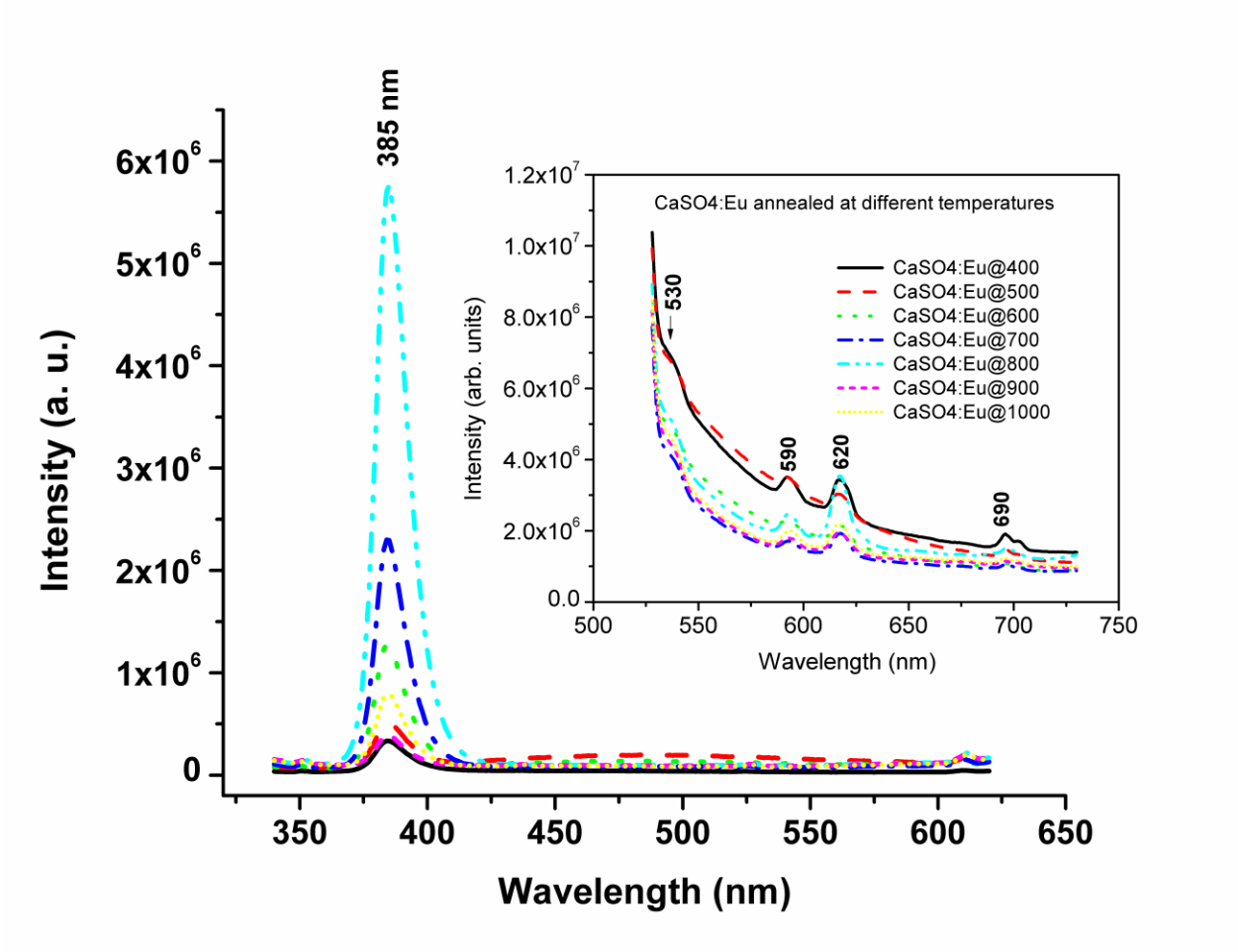

Fig. 10. Photoluminescence emission spectra of $CaSO_4$:Eu phosphor annealed at 900 ^oC (i.e., $CaSO_4$:Eu@900 phosphor and excited by 320 nm). Photoluminescence emission spectra (excited by 253 nm wavelength) of $CaSO_4$:Eu@900 phosphor, **(a)** unirradiated (curve a), **(b)** irradiated for 1 kGy dose (curve b).

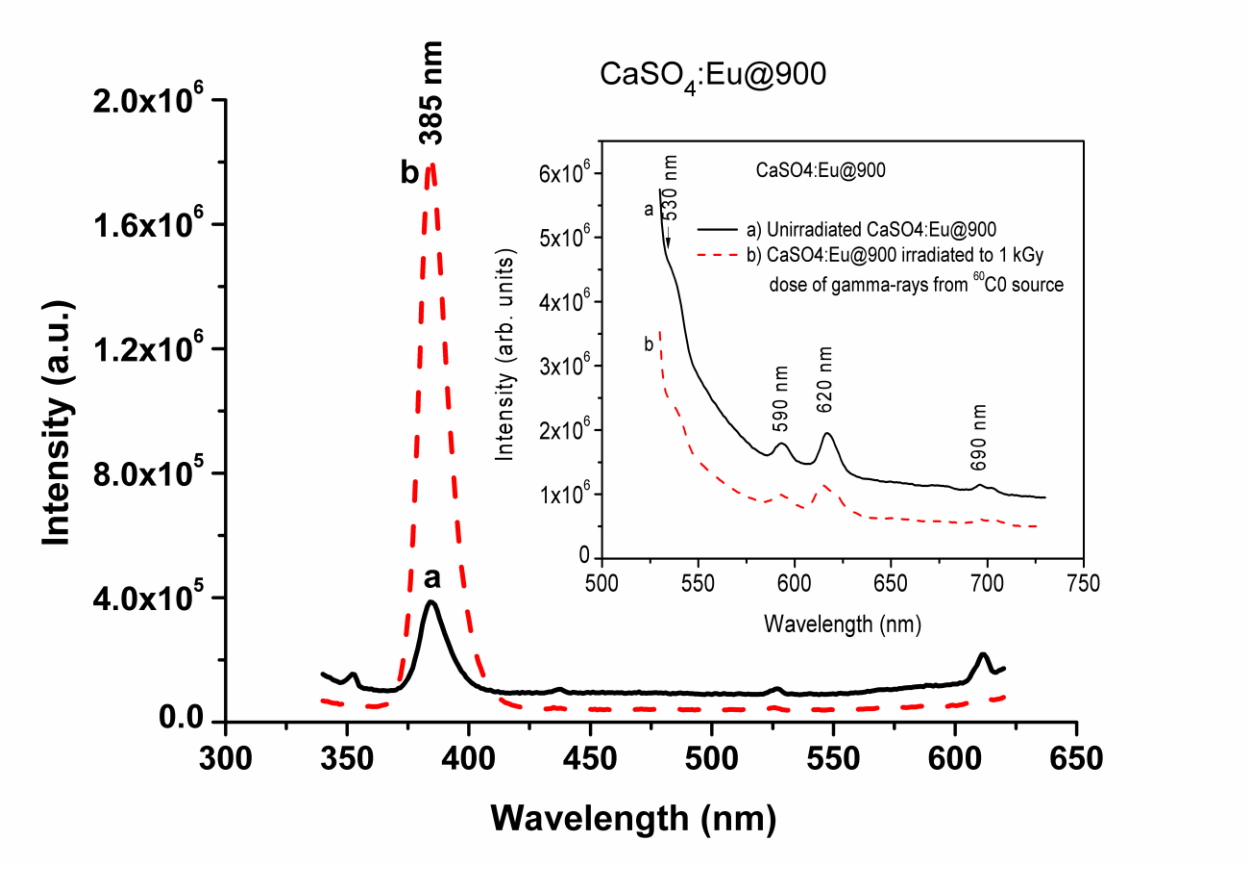

Fig. 11. OSL emission spectrum of the $CaSO_4$:Eu@900 sample stimulated by blue LED light (~470 nm, ~30 mW/cm^2 at the sample position). The OSL intensity (maximum intensity of the decay curve) is plotted with the wavelength of the narrow-band interference filters. The material was irradiated to 10 Gy from Sr^{90}/Y^{90} beta source. The OSL decay curves taken with the filters of different wavelengths are also shown in the inset for ready reference.

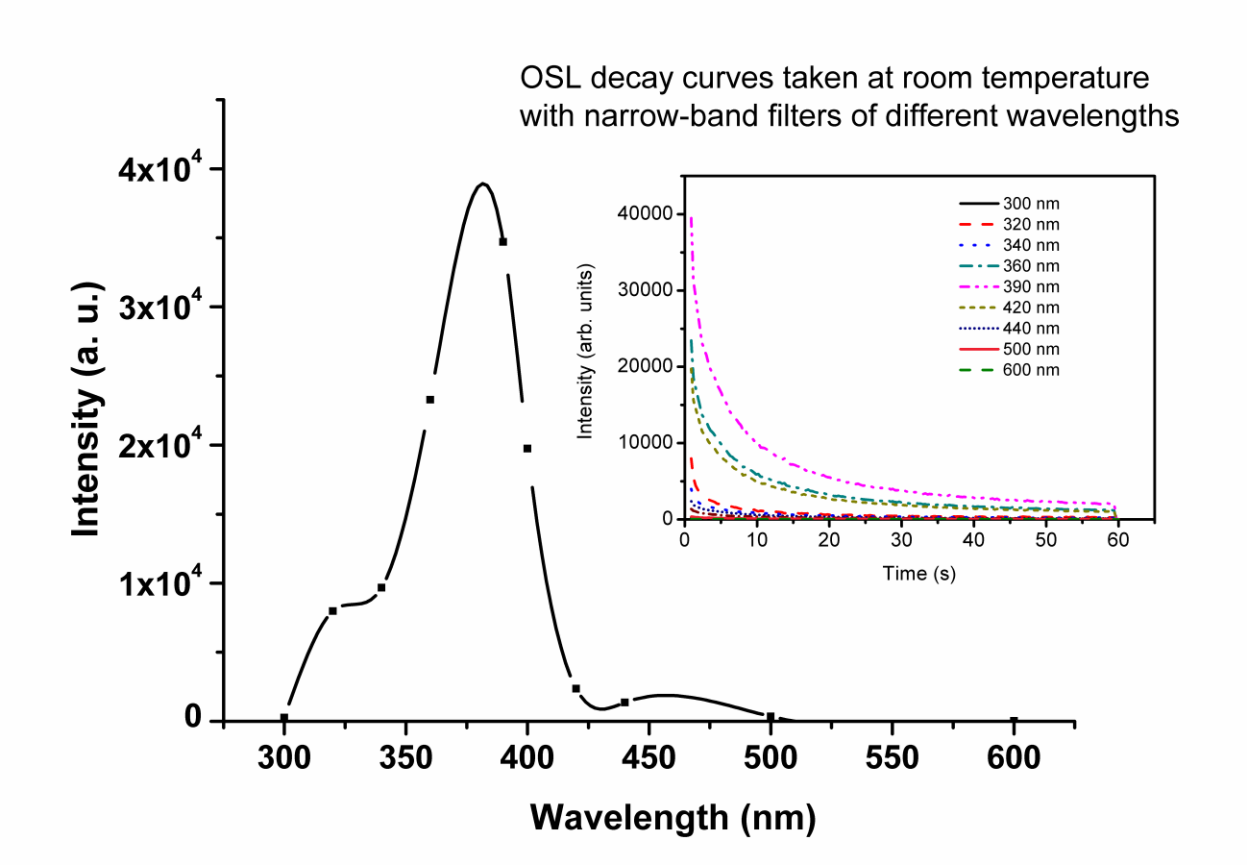

Fig. 12. Hexagonal 2×2×2 supercell model of **(a)** $CaSO_4$ and **(d)** $CaSO_4$:Eu with one Ca^{2+} substituted by Eu^{2+}. The calculated band structure and projected density of states (PDOS) for $CaSO_4$ (b & c) and $CaSO_4$:Eu (e & f). The Fermi energy is the zero of the energy scale.

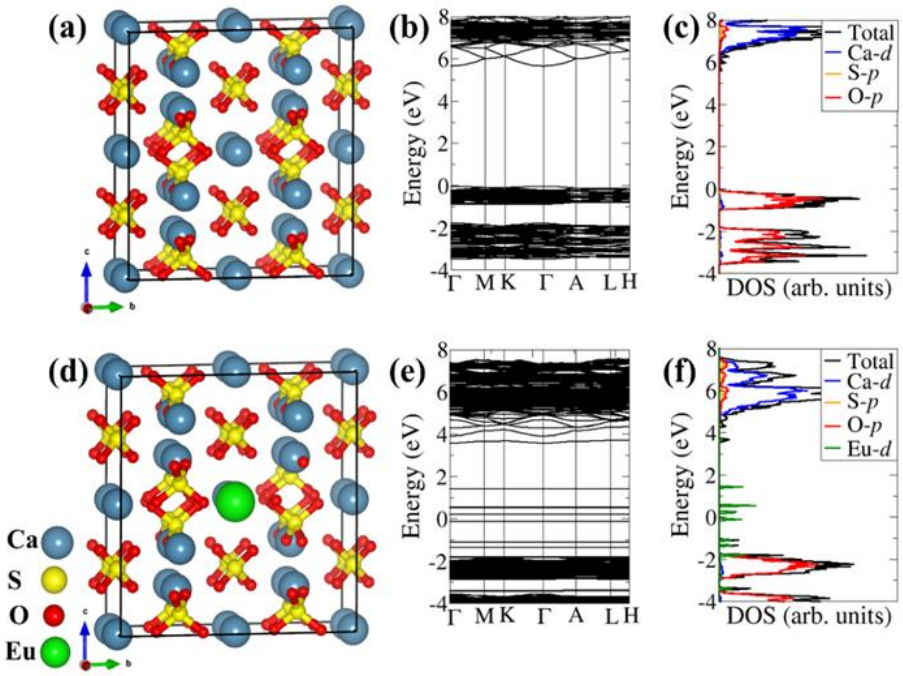

Fig. 13. Orthorhombic 2×2×2 supercell model of **(a)** $CaSO_4$ and **(d)** $CaSO_4$:Eu with one Ca^{2+} substituted by Eu^{2+}. The calculated band structure and projected density of states (PDOS) for $CaSO_4$ (b & c) and $CaSO_4$:Eu (e & f). The Fermi energy is the zero of the energy scale.